Characterization of a small tRNA -binding protein that interacts with the archaeal proteasome complex

Gaëlle Hogrel, Laura Marino-Puertas, Sébastien Laurent, Ziad Ibrahim, Jacques Covès, Eric Girard, Frank Gabel, Daphna Fenel, Marie-claire Daugeron, Béatrice Clouet-d'Orval, et al.

Received: 30 November 2020 | Revised: 15 May 2022 | Accepted: 17 May 2022

DOI: 10.1111/mmi.14948

RESEARCH ARTICLE

WILEY

Characterization of a small tRNA-binding protein that interacts with the archaeal proteasome complex

Gaëlle Hogrel[1] | Laura Marino-Puertas[1] | Sébastien Laurent[2] | Ziad Ibrahim[1] | Jacques Covès[1] | Eric Girard[1] | Frank Gabel[1] | Daphna Fenel[1] | Marie-Claire Daugeron[3] | Béatrice Clouet-d'Orval[4] | Tamara Basta[3] | Didier Flament[2] | Bruno Franzetti[1]

[1]CNRS, CEA, IBS, Univ Grenoble Alpes, Grenoble, France

[2]Laboratoire de Microbiologie des Environnements Extrêmes, Ifremer, CNRS, Univ Brest, Plouzané, France

[3]Institute for Integrative Biology of the Cell (I2BC), CEA, CNRS, Université Paris-Saclay, Gif-sur-Yvette, France

[4]Laboratoire de Microbiologie et de Génétique Moléculaires, UMR5100, Centre de Biologie Intégrative (CBI), Université de Toulouse, CNRS, Université Paul Sabatier, Toulouse, France

Correspondence
Bruno Franzetti, Extremophiles and Large Molecular Assemblies Group (ELMA) Institut de Biologie Structurale (IBS) CNRS/CEA/Grenoble-Alpes Univ. 71 avenue des martyrs 38000, Grenoble, France.
Email: bruno.franzetti@ibs.fr

Present address
Gaëlle Hogrel, University of St Andrews, St Andrews, UK

Ziad Ibrahim, University of Leicester, Leicester, UK

Funding information
Agence Nationale de la Recherche, Grant/Award Number: ANR-10-INBS-05-02, ANR-16-CE12-0016-01, ANR-17-EURE-0003, ANR-18-CE11-0018-01, CE12-0016-01 and CE11-0018-01; European Synchrotron Radiation Facility; Fondation pour la Recherche Médicale; FRISBI, Grant/Award Number: UMS 3518

Abstract

The proteasome system allows the elimination of functional or structurally impaired proteins. This includes the degradation of nascent peptides. In Archaea, how the proteasome complex interacts with the translational machinery remains to be described. Here, we characterized a small orphan protein, Q9UZY3 (UniProt ID), conserved in Thermococcales. The protein was identified in native pull-down experiments using the proteasome regulatory complex (proteasome-activating nucleotidase [PAN]) as bait. X-ray crystallography and small-angle X-ray scattering experiments revealed that the protein is monomeric and adopts a β-barrel core structure with an oligonucleotide/oligosaccharide-binding (OB)-fold, typically found in translation elongation factors. Mobility shift experiment showed that Q9UZY3 displays transfer ribonucleic acid (tRNA)-binding properties. Pull-downs, co-immunoprecipitation and isothermal titration calorimetry (ITC) studies revealed that Q9UZY3 interacts in vitro with PAN. Native pull-downs and proteomic analysis using different versions of Q9UZY3 showed that the protein interacts with the assembled PAN–20S proteasome machinery in *Pyrococcus abyssi* (Pa) cellular extracts. The protein was therefore named Pbp11, for Proteasome-Binding Protein of 11 kDa. Interestingly, the interaction network of Pbp11 also includes ribosomal proteins, tRNA-processing enzymes and exosome subunits dependent on Pbp11's N-terminal domain that was found to be essential for tRNA binding. Together these data suggest that Pbp11 participates in an interface between the proteasome and the translational machinery.

KEYWORDS
Archaea, OB-fold, proteasome, protein–protein interaction, ribosome-associated quality control, tRNA binding

Abbreviations: AP/MS, affinity purification/mass spectrometry; EF-Tu, elongation factor thermo unstable; ITC, isothermal titration calorimetry; OB-fold, oligonucleotide/oligosaccharide-binding fold; Pa, *Pyrococcus abyssi*; PAN, proteasome-activating nucleotidase; PbaB, proteasome activator; Pbp11, proteasome-binding protein; Ph, *Pyrococcus horikoshi*; RQC, ribosome quality complex; SAXS, small-angle X-ray scattering; SAMPs, small archaeal modifier proteins.

1 | INTRODUCTION

The proteasome represents the main protein degradation machinery in Eukarya and Archaea. This large molecular machine consists of a 20S peptidase core that associates with regulatory particles responsible for the specific recognition of target proteins, their energy-dependent unfolding and their translocation in the 20S complex (Majumder & Baumeister, 2019). In Eukarya, the proteasome substrate selection is mainly achieved by the covalent attachment of small ubiquitin modifiers on target proteins involving a complex E1–E2–E3 enzymatic cascade (Finley et al., 2004). Ubiquitinated protein recognition and deubiquitination are achieved by a subset of subunits forming the lid of the 19S proteasome regulatory particle (Finley & Prado, 2020). The proteasome is mainly responsible for proteostasis by determining the half-lives of proteins in the cytosol. It also controls fundamental biological functions by rapidly eliminating a variety of regulatory factors (Navon & Ciechanover, 2009). In addition, the proteasome plays a key role in proteome quality control and stress response by eliminating toxic misfolded or damaged proteins in the cytosol (Goldberg, 2003). In particular, co-translational ubiquitination and subsequent proteasome activity were proposed to be responsible for the degradation of defective ribosomal products (Wang et al., 2013).

Archaea possess an eukaryotic-like 20S proteasome exhibiting reduced complexity in terms of subunit composition but with a similar overall organization (Maupin-Furlow, 2013a). The substrate unfolding and translocation into the archaeal 20S catalytic core are completed by the proteasome-activating nucleotidase (PAN) AAA-ATPase complex (Majumder & Baumeister, 2019; Zwickl et al., 1999). PAN forms a ring complex made of six subunits that share 41%–45% sequence identity with the eukaryotic AAA-ATPases forming the base of the 19S proteasome regulatory particle. Cryo-electron microscopy (Cryo-EM) structure and small-angle scattering studies of the archaeal PAN–20S complex from *Archaeoglobus fulgidus* and *Methanocaldococcus jannaschii* provided important fundamental insights into the functional cycle of proteolytic ATPases underlining the highly dynamic nature of the PAN complex (Ibrahim et al., 2017; Mahieu et al., 2020; Majumder et al., 2019).

The physiological roles of the archaeal proteasomes remain poorly explored. Gene expression studies indicated that proteasome subunits accumulate during heat or salt environmental stresses (Chamieh et al., 2008), while a recent study demonstrated a role in the regulation of cell division (Risa et al., 2020). Ubiquitin-like modification (SAMPylation, urmylation) activities have been reported in Archaea (Anjum et al., 2015; Humbard et al., 2010). This pathway seems to be dependent on a family of ubiquitin-like molecules called Small Archaeal Modifier Proteins (SAMPs) (Maupin-Furlow, 2013b). In most Archaea, the pathway depends only on a single E1-like SAMP activator (Ranjan et al., 2011). Recently, a complete ubiquitination cascade composed of E1/E2/RING-E3 eukaryotic-like enzymes was discovered in the Aigarchaeota and the Asgard archaea superphyla (Hennell James et al., 2017). Despite this progress, little is known about the recognition mechanisms and processing of the conjugated proteins by archaeal proteasome systems. In particular, there is no evidence yet for the existence of PAN-interacting factors potentially responsible for an elaborate regulation of the archaeal proteasome.

In the present study, we searched for novel PAN-interacting proteins using the deep-sea model hyperthermophilic archaeon *Pyrococcus abyssi* (Pa). By using in vitro affinity purification, coupled with mass spectrometry (MS) analysis, we identified Q9UZY3 (UniProt ID), a small orphan protein of 11 kDa, as a putative proteasome partner. We confirmed by pull-down and co-immunoprecipitation experiments that Q9UZY3 physically interacts with the proteasome regulatory particle PAN. We also report proteomic, biochemical and structural data indicating that Q9UZY3 is a tRNA-binding protein closely related to the archaeal proteasome in Thermococcales. We therefore named it Pbp11, for Proteasome-Binding Protein of 11 kDa. The tRNA-binding capacity of Pbp11 is required for the formation of a protein-interaction network composed mainly of ribosomal proteins, components of the universal tRNA-processing machinery, in particular various tRNA modification enzymes, and the RNA exosome-degrading machinery. These data highlight Pbp11 as a protein candidate to be part of a previously unrecognized ribosome-associated quality control system in Archaea.

2 | RESULTS

2.1 | Identification of Q9UZY3 as a proteasome regulatory complex interactant

The archaeal AAA-ATPase PAN functions as a protein unfoldase and displays 20S proteasome-activating properties in vitro (Smith et al., 2011; Wilson et al., 2000). In Eukarya, the homologous complex (called regulatory particle) acts as a platform for the docking of proteins involved in the regulation of the proteolytic machinery. Whether such proteins exist in Archaea is currently unknown. Here, we used the purified and active (Figure S1) recombinant His-tagged *P. abyssi* PAN as a molecular bait to search for partners in *P. abyssi* cell extracts as described in Pluchon et al. (2013). We selected a small protein of 11 kDa (UniProt ID: Q9UZY3) for more detailed studies since it was unambiguously detected by mass spectrometry (MS) in triplicate assays and not in the negative controls. Q9UZY3 has no predicted function and BLAST (Basic Local Alignment Search Tool) searches indicated that homologous proteins are present in Thermococcales. The protein alignment of these orthologs (Figure 1a) shows a moderate degree of conservation except in the N-terminal region, which is predicted to be disordered (Kelley et al., 2015). To validate our preliminary interaction data, we first performed reverse pull-down experiments using different Q9UZY3 constructs as baits. We purified Q9UZY3 expressed with N- or C-terminal Histidine tag (Q9UZY3-Ntag, Q9UZY3-Ctag) and a variant lacking the first 20 amino acids (Q9UZY3-ΔN-Ctag) (Figure S2a). Recovered proteins were analyzed by western-blot using a PAN-specific antibody. The raw figures and quantified data are available in Figure S3. The presence of the native PAN protein was significantly

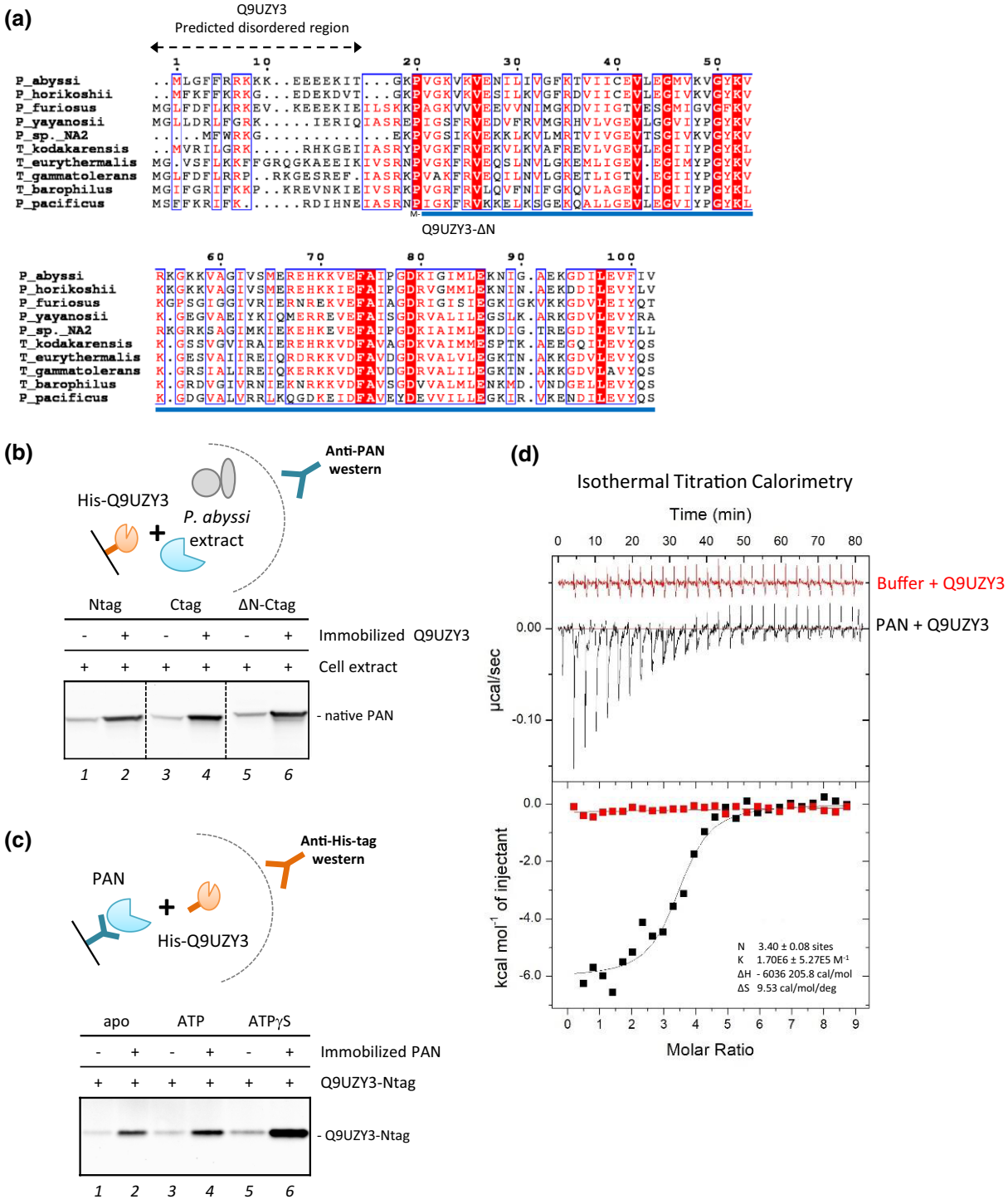

FIGURE 1 *Pyrococcus abyssi* Q9UZY3 physically interacts with PAN. (a) Q9UZY3 protein sequence alignment shows the amino acids' conservation for the core domain, while the disordered region (1–20) is poorly conserved. The blue line indicates the sequence corresponding to the N-ter truncated (ΔN) version of Q9UZY3. Details of the sequence alignment are provided in the materials and methods section. (b) Pull-down assays with immobilized His-tagged Q9UZY3. All three recombinant forms of Q9UZY3 (details in Figure S2a) co-precipitated PAN from *P. abyssi* cellular extract. Native *Pa*PAN was revealed by western-blot with anti-PAN antibodies. (c) Recombinant Q9UZY3-Ntag was co-purified with immobilized *Pa*PAN. Q9UZY3 was revealed by western-blot using anti-His-tag antibodies. The raw figures and quantified data are available in Figure S3. (d) Measurement of Q9UZY3 binding to *Pa*PAN by ITC at 45°C. Experimental data were fitted by one side binding model (in black) and buffer signal (in red) was substracted.

detected in the pull-downs of the three versions of recombinant Q9UZY3 (Figure 1b).

To determine if the pull-down that we detected in the total *P. abyssi* extracts corresponds to direct interactions between PAN and Q9UZY3, we performed in vitro interaction studies using purified recombinant proteins. We first performed co-immunoprecipitation experiments with purified proteins and showed that the untagged Q9UZY3 protein was efficiently captured by the immobilized PAN (Figure 1c). As an AAA-ATPase, PAN undergoes important conformational changes during the adenosine triphosphate (ATP) hydrolyzing cycle (Kim et al., 2015; Smith et al., 2011). The co-existing nucleotide states have been shown to be associated with modifications of the intersubunits' contact, rotation motions of the hexamer and binding to the 20S particle (Majumder et al., 2019). The co-immunoprecipitation experiments show that hydrolyzable ATP and non-hydrolyzable ATPγS (adenosine 5′-[γ-thio]-triphosphate) do not prevent the interaction between PAN and Q9UZY3 (Figure 1c). This last observation confirms the physical interaction of Q9UZY3 also with the nucleotide-binding form of PAN. Then, we tried to co-purify the PAN–Q9UZY3 complex using streptavidin-tagged Q9UZY3. PAN was co-eluted with Q9UZY3 after affinity column extensive wash and elution with biotin (Figure S4). However, the complex dissociated on size exclusion columns. We therefore used isothermal titration calorimetry (ITC) to quantify the binding equilibrium directly by measuring the heat change resulting from the association of Q9UZY3 to PAN. The ITC thermogram (Figure 1d) shows the titration of Q9UZY3 when injected into PAN solution. Fitted with a one binding site model, it allows one to determine a K_D value of 0.59 ± 0.18 μM.

To determine which PAN domains are important for the formation of the PAN–Q9UZY3 complex, we produced the N-terminal domain, responsible for substrate recognition (PAN1), and the ATPase-containing domain (PAN2) separately (Figure S5a). Because *Pa*PAN1 displayed a tendency to aggregate in solution, we chose to reconstitute the complex using *Pyrococcus horikoshii* (Ph) system, with *Ph*PAN1, *Ph*PAN2 being orthologous to *Pa*PAN1, *Pa*PAN2, and O58951 to Q9UZY3. Co-immunoprecipitation assays not only confirmed that the interaction is conserved in another species (Figure S5b, lane 4) but also revealed that Q9UZY3 ortholog specifically binds *Ph*PAN2 (Figure S5c, lane 8) and not *Ph*PAN1. Interestingly, the N-terminal region of Q9UZY3, predicted to be disordered, is not essential for Q9UZY3 complex formation with PAN (Figure 1b, lane 6). Collectively, these experiments strongly support direct interactions between PAN and Q9UZY3 in vitro and suggest the existence of a physiological complex between these proteins. We then performed enzymatic assays to explore whether Q9ZUY3 can regulate PAN unfoldase activity. However, unfolding kinetics of the fluorescent substrate, GFPssrA, in the presence of PAN did not show significant effect of Q9UZY3 on this activity (Figure S6a). The subunits of the *P. abyssi* 20S complex (α, β1, β2) were purified and assembled (Figure S6b) to assess if the PAN:20S could degrade Q9UZY3. The signal of the GFPssrA was followed by western blot as positive control for PAN–20S activity (Figure S6c). In vitro previous studies reported proteolytic activity of the 20S complex without the regulatory particle PAN (Anjum et al., 2015), as observed here with the GFPssrA as substrate (Figure S6c, lane 3). But, in the same conditions, no significant degradation of Q9UZY3 by the 20S proteasome in the absence or presence of PAN could be observed (Figure S6d). At this stage of the study, we did not detect, in our conditions, any functional interaction with PAN. We analyzed then the structural properties of Q9UZY3 to gain further insight into its function.

2.2 | The crystal structure of Q9UZY3 reveals similarities with nucleic-acid binding modules

The X-ray structure of the Q9UZY3 ortholog from *Pyrococcus furiosus* (*Pf*) (77% sequence identity) was deposited in the Protein Data Bank (PDB code: 1XE1 and 4PGO), but no further characterization was published. Using the Q9UZY3-ΔN-Ctag construct from *P. abyssi*, we obtained crystals and solved the structure by molecular replacement at a resolution of 1.65 Å (Figure 2a PDB: 7ANU, Table S3). Despite a moderate sequence identity between the Q9UZY3 proteins from *P. furiosus* and *P. abyssi*, the X-ray structure of Q9UZY3 is remarkably well conserved (root mean square deviation [RMSD] = 0.466 Å, for 58 residues).

In order to investigate the shape of the protein in solution, we performed small-angle X-ray scattering (SAXS) analysis of Q9UZY3 (see acquisition parameters Table S4). An excellent fit (χ^2 = 1.07) was obtained between the experimental curve of Q9UZY3-ΔN-Ctag and the theoretical curve calculated from the X-ray crystal structure when considering the Q9UZY3 as a monomer (Figure S7a). Using the Bayesian inference (Hajizadeh et al., 2018) from the ATSAS suite (Franke et al., 2017), the molecular weight interval was predicted within the interval 7950–9950 Da for a theoretical value of 10,200 Da. Together, these data confirm that Q9UZY3-ΔN-Ctag is a monomeric protein in solution. Guinier analysis of the experimental SAXS curve of Q9UZY3-Ctag yielded a radius of gyration (Rg) of 17.3 Å (Figure S7b). Here, the Bayesian inference calculated a molecular weight interval of 10,850–12,400 Da for a theoretical molecular weight of 12,509 Da. Based on these data and supported by the gel filtration profile (Figure S2), the full-length (FL) Q9UZY3 behaves also mainly as a monomeric protein in our conditions.

From the structural analysis, we noticed that Q9UZY3 main core (Figure 2a) is reminiscent of the oligonucleotide/oligosaccharide-binding (OB)-fold domain (Murzin, 1993), known to bind nucleic acids (Arcus, 2002; Theobald et al., 2003). The OB-folds have a low degree of sequence or structural similarity, but they are typically formed of five-stranded β barrels with interspersed loop and helical elements (Figure S8a). Q9UZY3 also displays β-barrel architecture; it is composed of six β-sheets connected by loops and lacks α helices, suggesting that it may be a non-canonical OB-fold protein.

We next searched for structural homologs of Q9UZY3 using the DALI server (Holm, 2020). Surprisingly, this search retrieved classical translation elongation factors such as elongation factor thermo unstable (EF-Tu) (Bacteria) and elongation factor 1-alpha (EF-1α)

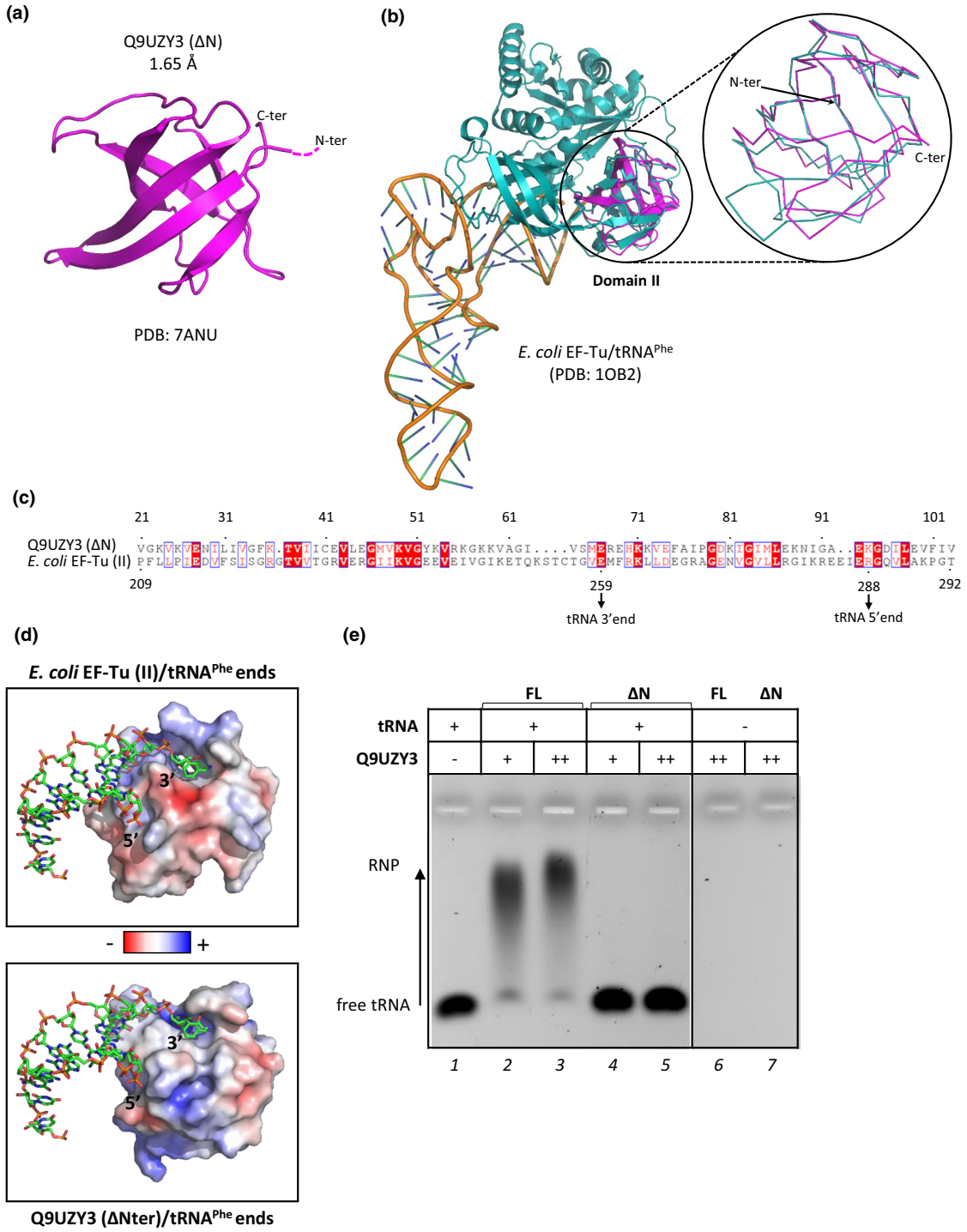

FIGURE 2 The archaeal Q9UZY3 displays features of a transfer ribonucleic acid (tRNA)-binding protein. (a) X-ray structure of Q9UZY3 protein determined at a resolution of 1.65 Å displays an oligonucleotide/oligosaccharide-binding fold (OB-fold)-like domain (PDB: 7ANU). The missing N-terminal tail is indicated by a dotted line. (b) Q9UZY3 shares structural homology with the domain II of translation elongation factors. Left panel, representation of elongation factor thermo unstable (EF-Tu) from *Escherichia coli* (*Ec*) (in cyan) complexed with $tRNA^{Phe}$ (1OB2) and aligned with Q9UZY3 (in magenta). Right circle, backbone representation of Q9UZY3 (in magenta) aligned with the domain II of *Ec*EF-Tu (1OB2) (in cyan). (c) Sequence alignment of Q9UZY3 with the domain II of *Ec*EF-Tu. Key residues involved in the binding of tRNA ends are indicated. (d) Electrostatic surface of *Ec*EF-Tu (II) (upper panel) and Q9UZY3 (lower panel). $tRNA^{Phe}$ was modeled into Q9UZY3 structure using the structural alignment with *Ec*EF-Tu (II) (1OB2). The surfaces were calculated with Adaptive Poisson–Boltzmann Solver (APBS) (Holst & Saied, 1993). In red, negatively charged surface (−5 kT/e); in blue, positively charged surface (+5 kT/e). (e) Electrophoretic mobility shift assays with tRNAs. Full-Length (FL) and N-ter truncated (ΔNQ9UZY3 were incubated at a molar ratio of 1:1 (lanes 2, 4) or 2:1 (lanes 3, 5) with *Pyrococcus abyssi* (*P. abyssi*) tRNAs. Samples were loaded to 0.8% agarose gel and ribonucleoprotein complexes (RNP) were revealed by staining with ethidium bromide. Lanes 6 and 7: proteins were loaded in the absence of added tRNA as negative control for a nucleic-acid signal.

(Eukarya/Archaea) as most significant hits. To further explore the similarity with translation elongation factors, we superimposed the structure of Q9UZY3 with the one of *Escherichia coli* (*E. coli* [*Ec*]) EF-Tu (*Ec*EF-Tu) bound to $tRNA^{Phe}$ (Figure 2b). Significant root mean square deviation (RMSD) score (1.04 Å, over 55 amino acids, Coot [Emsley et al., 2010]) was obtained supporting structural homology with the domain II of *Ec*EF-Tu (*Ec*EF-Tu II). To confirm, we aligned the Q9UZY3 structure with several translation elongation factors (Figure S8b). All alignments fitted into the second domain with significant RMSD scores.

Domain II of EF-Tu interacts specifically with tRNA ends through conserved amino acids, such as E259 and R288, in *Ec*EF-Tu (Nissen et al., 1999), and contains a pocket suitable for the aminoacylated 3′ end (Nissen et al., 1995; Figure 2d, upper panel). Intriguingly, the two amino acids involved in tRNA end interaction are conserved between *Ec*EF-Tu II and Q9UZY3 (Figure 2c). Moreover, after overlaying the electrostatic surface of Q9UZY3 with *Ec*EF-Tu II–tRNA complex, we noticed that Q9UZY3 also contains a slightly positively charged pocket for the 3′CCA end charged with the amino acid (Figure 2d, lower panel). Together these data suggest that Q9UZY3 is a tRNA-binding protein, which might recognize the acceptor stem extremity of tRNAs.

2.3 | Q9UZY3 specifically binds tRNAs

To assess if Q9UZY3 binds tRNA as suggested by structural homology with *Ec*EF-Tu II, we performed electrophoretic mobility shift assays using total tRNAs extracted from *P. abyssi* (Figure 2e). We observed a specific gel shift retardation mirroring the formation of a ribonucleoprotein complex (RNP) by the addition of full-length Q9UZY3 to the reaction mixture (Figure 2e, lanes 1 to 3). No shift was observed by using the truncated version of Q9UZY3 at the N-terminus (ΔN) (Figure 2e, lanes 4 and 5). Therefore, the N-terminal domain is essential for the RNA-binding capacity of Q9UZY3. These results were reproducible with the different Q9UZY3 constructs (Figure S9). Similar experiments with short single-stranded DNA/RNA, double-stranded DNA or DNA/RNA hybrid did not allow to detect gel shift retardation (Figure S10). In the light of our data, we propose that Q9UZY3 is able to bind tRNAs and that flexible N-terminal tail is required for the binding.

2.4 | The Q9UZY3 interaction network connects the proteasome with ribosome and ribosome-associated machinery

To identify the proteins interacting with Q9UZY3 from the *P. abyssi* cell extract, we used Q9UZY3 recombinant protein as a bait in an N- or C-terminal His-tagged version and performed affinity purification coupled to mass-spectrometry (AP/MS) analyses. In parallel, control experiments without bait protein were carried out to eliminate unspecific proteins from our analysis. Similar assays were performed with a nuclease treatment to reduce RNA- or DNA-mediated Q9UZY3 interactions. We specifically identified 45 protein partners retrieved with both tagged versions of the bait protein (Figure 3a). Among them, 11 were still detected after nuclease treatment (Figure 3b).

Assignments of Gene Ontology (GO) terms (Ashburner et al., 2000; The Gene Ontology Consortium, 2019) of each candidate (Table S4) confirm that Q9UZY3 is, as expected, closely connected to the proteasome degradation pathway (Figure 3, orange). In addition to PAN, all 20S proteasome subunits (α, β_1 and β_2) were identified, suggesting that Q9UZY3 interacts with the assembled PAN–20S proteasome core complex. Moreover, a less known archaeal proteasome activator was also retrieved, PbaB, which was reported to function as an ATP-independent proteasome activator and a molecular chaperone in *P. furiosus* (Kumoi et al., 2013). The same experiment with the ΔN version of Q9UZY3 as a bait reaffirmed the connection with the proteasome machinery with five out of seven partners annotated as proteasome subunits (Figure 3c). In addition, Q9V1Q0, homologous to the aminopeptidase TET1 which is a proteolysis-related protein (Durá et al., 2005), was identified. This factor is supposed to be involved in the trimming of proteasome degradation products (Borissenko & Groll, 2005). Nevertheless, its detection in the Q9UZY3 network was dependent on the presence of the N-terminal domain.

Remarkably, besides the proteasome system, 55% of the Q9UZY3 network is composed of partners with assigned function in RNA metabolism (Figure 3a, ribosomal proteins, tRNA modification proteins, RNA catabolic process). Several ribosomal subunits of both 30S and 50S subunits, two components of the RNA exosome as well as the recently described 5′-3′ exoribonuclease aRNase J and the RNA helicase ASH-Ski2 (Phung et al., 2020) are specifically detected. Interestingly, most of these partners are missing from both the nuclease-treated (Figure 3b) and the ΔN version (Figure 3c) networks. These data strongly suggest that the connection to partners in RNA metabolism occurs via RNA and requires the RNA-binding capacity of Q9UZY3 as described above (Figure 2e).

The molecular identity of the Q9UZY3 natural partners determined in the interactomes is in good agreement with the in vitro PAN and RNA-binding activities that we described. Accordingly, we propose to name it Pbp11 for Proteasome-Binding Protein of 11 kDa. The loss of the RNA-related protein partners in the interactomes when the samples were treated with RNAse or when the Q9UZY3 RNA-binding function was abolished also corroborates the RNA-binding activity of Pbp11.

3 | DISCUSSION

Protein degradation processes must be both efficient and tightly regulated to ensure protein homeostasis. In Archaea, little is known about recognition mechanisms of the conjugated proteins by the proteasome system or how it could be connected to other fundamental

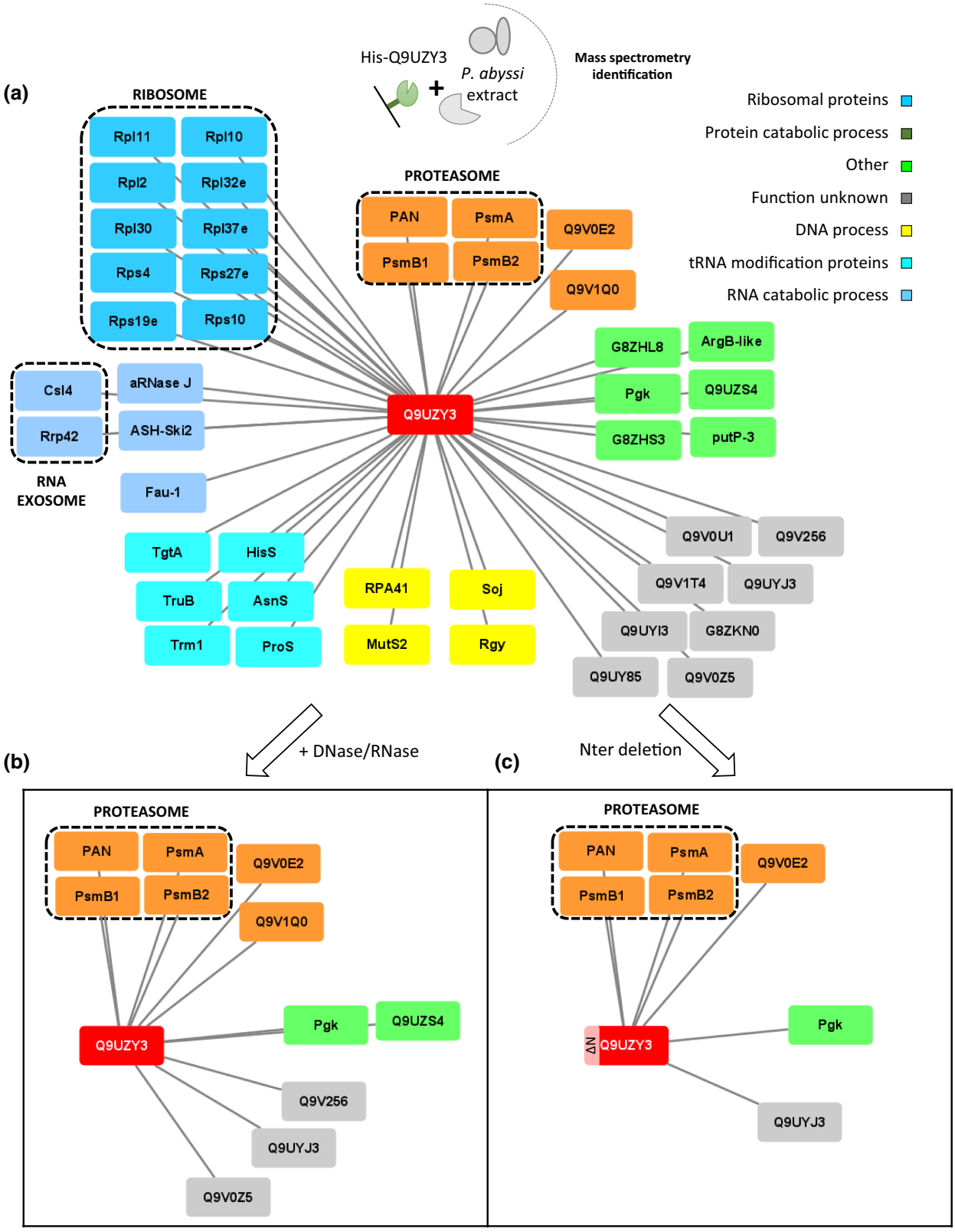

FIGURE 3 Protein–protein interaction network of *Pyrococcus abyssi* (*P. abyssi*) Q9UZY3. (a) Q9UZY3 network displayed with Cytoscape 3.7.2 software (Shannon et al., 2003). The full partner list is presented in Table S4 following biological process classification. Q9UZY3 partners were significantly captured by both His-tag variants as described in the materials and methods section. These data are the result of four experimental replicates. (b) Remaining Q9UZY3 network after (ribo)nuclease treatment. These data are the result of four experimental replicates. (c) Core network of Q9UZY3. Protein partners retrieved both in the Q9UZY3 network (a) and in the network of Q9UZY3-ΔN. These data are the result of duplicates. Subunits of described macromolecular machinery are framed in a black dotted line.

processes. The regulation of the 20S archaeal proteasome is supposed to be principally assumed by the hexameric AAA-ATPase PAN. This protein is responsible for targeting misfolded proteins, for opening the 20S α-ring and for unfolding and translocating the polypeptide chain into the proteolytic chamber. To date, there is no evidence for the existence of PAN-interacting factors possibly responsible for regulation of the archaeal proteasome.

In this work, we identified a unique small protein that interacts with the proteasome machinery, which we named Pbp11 (UniProt ID, Q9UZY3). Remarkably, we show that Pbp11 has the ability to bind to tRNAs extracted from *P. abyssi* and is conserved among Thermococcales. Pull-down experiments using total *P. abyssi* protein extract, co-immunoprecipitation and co-purification using purified recombinant proteins highlighted a strong connection between Pbp11 and PAN. The presence of the proteasome activator, PbaB, and the aminopeptidase TET1, a large peptidase complex that processes 20S protease–peptide products, in the Pbp11 interaction network suggests the capture of an active protein-degrading system able to unfold protein substrate until their degradation into amino acids (Groll et al., 2003; Kusmierczyk et al., 2011).

Our observations also let us to question whether Pbp11 could function as a targeting signal for the degradation of a specific protein class associated with tRNA. In Archaea, proteins named SAMPs with structural (but no sequence) similarity to eukaryotic ubiquitin are widely distributed across the archaeal phyla (Maupin-Furlow, 2011). In *Sulfolobus acidocaldarius*, SAMP orthologs have been shown to function as targeting signals for the degradation by the PAN–20S complex (Anjum et al., 2015). In *P. abyssi*, Q9UYT7 and Q9V034 are annotated as SAMP homologs but they were not found in the Pbp11 interaction network. Here, Pbp11 does not contain the canonical C-terminal di-glycine motif used for the covalent attachment of ubiquitin-like modifiers to target proteins (Burroughs et al., 2007). Moreover, no physical interaction was observed between Pbp11 and PAN N-terminal coiled coils involved in protein substrate recognition. Altogether, this argues against the direct function of Pbp11 in proteolysis pathways as a small modifier protein like SAMP/Urm1 proteins. Moreover, we could not detect a significant proteolytic activity of the PAN–20S system on the small Pbp11 protein. Together these observations suggest that Pbp11 is unlikely a substrate of the PAN-proteasome. However, one cannot completely exclude that in vivo, Pbp11 could be a long-lasting substrate of the proteasome.

A remarkable property of the Pbp11 protein, revealed by our structural and biochemical analyses, is its capacity to bind tRNAs extracted from *P. abyssi*. In addition, the Pbp11 interaction network includes tRNA-modifying enzymes or constituent proteins of tRNA-binding complexes such as ribosomal proteins. It is interesting to note that these partners, unlike the proteasome machinery, are lost after degradation of the RNA in the cell extract or in the absence of the Pbp11 N-terminal domain binding the tRNA. These observations indicate that the tRNA-binding properties of Pbp11 could be harnessed to target the proteasome activity toward tRNA-containing complexes. A molecular cross-talk between the proteasome, ribosome and RNA-degrading machinery has been described in Eukarya in the context of the translational-associated quality control (Karamyshev & Karamysheva, 2018; Sha et al., 2009). The stalled ribosomes act as a signal for ribosome recycling and for the destruction of nascent peptide by the 26S proteasome system (Dimitrova et al., 2009; Ito-Harashima et al., 2007; van Hoof et al., 2002). The eukaryotic ribosome-associated protein quality control (ribosome quality complex [RQC]) system involves a multiprotein complex that includes a specific E3 ligase to trigger the ubiquitinylation of nascent peptides (Defenouillère & Fromont-Racine, 2017; Doamekpor et al., 2016). The RQC binds stalled 60S ribosomal particles and the ubiquitinated defective translation products are subsequently transferred to the proteasome by the cell division control protein 48 (CDC48) AAA-ATPase complex (Defenouillère et al., 2013). The pathways that control protein- and RNA-quality are particularly important to eliminate defective elongation products generated by stress conditions or by aberrant non-stop or no-go messenger RNAs (mRNAs) to maintain proteostasis (Doma & Parker, 2006; Frischmeyer et al., 2002). Concomitantly, the RNA exosome quality control system is recruited to process defective mRNAs or ribosomal RNAs (rRNAs). Two decades ago, based on comparative genomics analyses, Koonin and colleagues proposed a tight functional coupling between translation, RNA processing and degradation (mediated by the exosome) and protein degradation (mediated by the proteasome) in Archaea (Koonin et al., 2001). Here, the existence of archaeal proteins, homologous to some members of the eukaryotic RQC system and the connection between ribosome, exosome and proteasome revealed in this study, suggests the existence of a RQC system in Archaea. Some proteins with unknown functions retrieved in the Pbp11 interaction network provide a starting point in the search for components of the archaeal RQC. A promising candidate is Q9V0U1 protein, as it shares 33% sequence identity (56% similarity) with Rqc2 homolog from *Haloferax volcanii* and displays NEMF-bacterial FbpA (fibronectin-binding protein A)-like proteins, Caliban and Tae2 (NFACT) domain typical for Rqc2 proteins (Lytvynenko et al., 2019; Figure S11).

One important remaining question is to understand whether Pbp11 is a Thermococcales-specific protein that was acquired in response to chaotropic environmental conditions or whether it is more widely spread among (extremophilic) Archaea. The sequence-based search for orthologs outside Thermococcales was hindered by the small protein size of Pbp11 and its low sequence conservation even among closely related Thermococcales species. We therefore cannot exclude the existence of Pbp11 orthologs in other Archaea.

In conclusion, the results described in this study lead us to propose Pbp11 as an interesting candidate to study tight connections between the proteasome complex and RNA-processing machinerys through its interaction with tRNAs. It remains to be determined how, mechanistically, Pbp11 could participate in the physical connection between these nanomachines in the context of extremophilic Archaea.

4 | MATERIALS AND METHODS

4.1 | Protein sequence alignment

Amino acid sequences from *Pyrococcus abyssi* (Q9UZY3), *Pyrococcus horikoshii* (O58951), *Pyrococcus furiosus* (Q8U2D2), *Pyrococcus yayanosii* (F8AH42), *Pyrococcus sp. NA2* (F4HKB3), *Thermococcus kodakarensis* (Q5JIQ5), *Thermococcus eurythermalis* (A0A097QT95), *Thermococcus gammatolerans* (C5A299), *Thermococcus barophilus* (A0A0S1XFW4) and *Paleococcus pacificus* (A0A075LPX0) were aligned with the T-coffee package (Di Tommaso et al., 2011; Notredame et al., 2000) and viewed with ESPript 3.0 (Robert & Gouet, 2014). The N-terminal region was predicted as disordered by secondary structure analysis with Phyre 2 (Kelley et al., 2015).

4.2 | Protein purification

4.2.1 | PAN

A truncated form of PAN from *P. abyssi* (PaPAN, UniProt: Q9V287), lacking the first 31 amino acids (Figure S1), was synthesized and cloned into pET-30a(+) vector (Genecust), between the NdeI and NotI restriction sites, to promote the expression of the protein of interest with a 6-Histidine tag at the C-terminal position. PaPAN was overexpressed in *E. coli* BL21(DE3) cells carrying PAN/pET-30a(+). IPTG (isopropyl-1-thio-D-galactopyranoside) was added to a final concentration of 1 mM, and the cells were further grown overnight at 20°C to induce the expression from PAN/pET-30a(+). The cells were harvested by centrifugation at 3000×*g* for 15 min. The cell pellet was resuspended into Buffer 1 (50 mM Tris–HCl, pH 8.0, 150 mM KCl, 150 mM NaCl, 10 mM $MgCl_2$, 10% glycerol), complemented with 0.25 mg ml^{-1} lysozyme (Euromedex), 0.05 mg ml^{-1} DNase I grade II (Roche), 1 mg ml^{-1} Pefabloc SC (Roche) and ethylenediaminetetraacetic acid (EDTA)-free protease inhibitor (cOmplete™, Roche). The cell pellet was mixed and incubated for 30 min at 4°C and then, was disrupted by using a LM20 Microfluidizer (Microfluidics) covered in ice at 18 KPsi (kilo-pound per square inch). Then, the lysate was incubated at 80°C for 10 min and centrifuged at 10,000×*g* for 1 h.

The soluble fraction was loaded into an affinity column (5 ml-HiTrap Chelating HP, GE Healthcare) equilibrated with Buffer 1 supplemented with 20 mM imidazole. After washing with 40 mM imidazole, the protein was eluted with Buffer 1, supplemented with 300 mM imidazole. Then, the buffer was exchanged by dialysis (10 MWCO (molecular weight cut-off) to 20 mM Tris–HCl, pH 8.0, and 150 mM NaCl. The protein was loaded onto an anion exchange column (Resource Q, GE Healthcare) and was eluted with 20 mM Tris–HCl, pH 8.0, and a linear salt gradient (0.15–1 M NaCl). Next, PAN was injected into the gel filtration column (Superdex 200 10/300 GL, GE Healthcare). The elution buffer was composed of 20 mM Tris–HCl, pH 8.0, 150 mM KCl, 150 mM NaCl, 10 mM $MgCl_2$ and 1 mM dithiothreitol (DTT).

The final PAN concentration was calculated by measuring the absorbance at 280 nm with a predicted extinction coefficient of 14,440 M^{-1} cm^{-1} and a molecular weight of 254,231.4 Da (for the hexameric PAN) (ProtParam, ExPASy; Gasteiger et al., 2005).

4.2.2 | Q9UZY3 (Pbp11)

Four recombinant versions of *P. abyssi* Q9UZY3 were synthesized and cloned (Genecust) as described in Figure S2. Following the same protocol as for PAN expression, proteins were overexpressed in *E. coli* BL21(DE3) and cell pellets were resuspended into Buffer 2 (20 mM Tris–HCl, pH 8.0, 150 mM NaCl), complemented with 0.1% Triton X-100, 25 mM $MgSO_4$, 0.25 mg ml^{-1} lysozyme (Euromedex), 0.05 mg ml^{-1} DNase I grade II (Roche), 0.2 mg ml^{-1} RNase (Roche) and EDTA-free protease inhibitor (cOmplete™, Roche). The cells were disrupted by sonication and incubated at 25°C for 30 min. Then the cell extract was treated by heating at 70°C for 15 min and the lysate was clarified by centrifugation at 10,000×*g* for 1 h. His-tagged Q9UZY3 was purified by using (i) an affinity column (5-ml HiTrap Chelating, GE Healthcare) with a linear gradient of 20–250 mM imidazole; (ii) a cation exchange column (Resource S, GE Healthcare) with a linear gradient of 50–500 mM NaCl and (iii) a size exclusion column (Superose 12, GE Healthcare) with elution in Buffer 2. For the untagged Q9UZY3, only the purification steps (ii) and (iii) were performed. The final Q9UZY3 concentration was calculated by measuring the absorbance at 280 nm using the predicted extinction coefficient (ProtParam, ExPASy) listed in Table S1. The primers and cloning strategies for expression in bacteria cells are listed in Table S2.

4.3 | Isothermal titration calorimetry (ITC)

ITC measurements were carried out at 45°C with a 250 rpm (revolutions per minute) stirring with the MicroCal PEAQ-ITC (Malvern Panalytical). A 200-µl sample of 7.9 µM PaPAN in ITC buffer (20 mM Tris–HCl, pH 8.0, 150 mM NaCl, 150 mM KCl, 10 mM MgCl, 1 mM DTT) was titrated with 2 µl injections of a total of 27 (2 µl × 27 injections) of 324 µM Q9UZY3-Ctag-His in ITC buffer in 5 s each injection at 180 s intervals. Curve was fitted by a one binding site model and the buffer signal was subtracted.

4.4 | Protein crystallization and data processing

Initial screening for crystallization conditions of the truncated Q9UZY3-ΔN-Ctag (Figure S2) was performed at the HTX Lab platform (EMBL, Grenoble, France). According to initial crystal hits obtained, the conditions were manually optimized by vapor diffusion at 293 K. A 1.5 µl drop of protein solution (20 mM Tris–HCl, pH 8.0, 150 mM NaCl), concentrated at 11 mg ml^{-1}, was mixed with 1.5 µl of solution containing 200 mM potassium thiocyanate

and 25% polyethylene glycol (PEG) 3350. After 2 days, crystals were harvested, soaked in the previous crystallization solution supplemented with 20% glycerol and finally cryo-cooled in liquid nitrogen.

Q9UZY3-ΔN-Ctag diffraction data were collected on a single crystal at the ID23 beamline of the European Synchrotron Radiation Facility (ESRF, Grenoble, France). Diffraction frames were integrated using the program XDS (Kabsch, 2010). Scaling, molecular replacement and density modification were done within the CCP4 suite of programs (McCoy et al., 2007) using SCALA (Evans, 2006), PHASER (McCoy et al., 2007) and DM (Cowtan & Zhang, 1999), respectively. The structure of *Pyrococcus furiosus* Pbp11 ortholog (RCSB PDB accession code: 1XE1) was used as search model for molecular replacement. Automatic model building was performed with the program BUCCANEER (Cowtan, 2006). Then the initial model was manually improved in Coot (Emsley et al., 2010) prior to refinement with PHENIX (Adams et al., 2010). Two units of Q9UZY3 were found in the asymmetric unit, likely stacked within their respective hexahistidine tag through the binding of a nickel ion.

Data collection and refinement statistics are summarized in Table S3. Structural figures were prepared with PyMOL (The PyMOL Molecular Graphics System, Version 1.3 Schrödinger, LLC).

4.5 | tRNA-binding electrophoretic mobility shift assays

Pyrococcus abyssi cells were grown overnight at 95°C in 50 ml of yeast extract, peptone and sucrose (YPS) medium under anaerobic conditions as described earlier (Erauso et al., 1993). Cells were collected by centrifugation (5000×*g*, 10 min) at 4°C and total tRNAs were extracted using Trizol (Sigma-Aldrich) and purified on 8 M urea acrylamide gel as described (Perrochia et al., 2013). Next, 30 μM tRNA (0.9 $\mu g \mu l^{-1}$) was incubated with 36 or 72 μM of Q9UZY3 recombinant protein in buffer containing 20 mM Tris–HCl, pH 8.0, 50 $\mu g ml^{-1}$ bovine serum albumin (BSA), 2 mM DTT, 0.5% Triton and 300 mM NaCl. Samples were incubated on ice for 15 min, loaded onto a 0.8% (w/v) agarose gel and separated by electrophoresis at 4°C in 1× TBE (Tris-borate-EDTA) buffer. Ribonucleoprotein complexes (RNP) were revealed after staining with ethidium bromide solution (0.5 $\mu g ml^{-1}$).

4.6 | Cell extract preparation

Pyrococcus abyssi was cultivated on exponential growth phase in bioreactors under physiological conditions (95°C, pH 6.5, anaerobic). The cell extracts were prepared as described (Pluchon et al., 2013). Briefly, *P. abyssi* pelleted cells were resuspended in 1/3 w/v of 1× phosphate-buffered saline (PBS) buffer (Euromedex), supplemented with EDTA-free protease inhibitor (cOmplete™, Roche). After sonication, the crude extracts were clarified by two successive centrifugations at 10,000×*g* for 60 min. The concentrations of total protein were measured by the Bradford protein assay (Bio-Rad).

4.7 | Pull-down experiments

Purified His-tagged Q9UZY3 were used as baits in the clarified whole-cell extract of *P. abyssi*. In a reaction volume of 200 μl supplemented with 10 mM $MgCl_2$, 20 μg of bait proteins was incubated overnight with 1 mg of *P. abyssi* extract under rotation at 4°C. The bait–extract complex was further incubated with 0.4 mg of cobalt-coated magnetic beads (Dynabeads, Invitrogen) for 3 h at 4°C and then washed three times with PBS buffer at 4°C.

To study the physical interaction between purified proteins, PAN and Q9UZY3, 8.33 μg of anti-*Pyrococcus horikoshii* PAN polyclonal antibody was immobilized onto 1.5 mg of magnetic Dynabeads Protein A (Thermo Fischer Scientific) in a final volume of 50 μl. Then, antibodies were covalently anchored using 29 μg of BS_3 crosslinker (Thermo Fischer Scientific). In a 20 μl reaction volume, 1 μg PAN was incubated with 2 μg Q9UZY3 for 15 min at 65°C first then at 4°C for 45 min in the binding buffer: 20 mM Tris–HCl, pH 8.0, 300 mM NaCl, 10 mM $MgCl_2$ and, when indicated, 4 mM ATP or 4 mM ATPγS (Figure 1c). The resulting protein complexes were trapped by anti-PAN Dynabeads over 15 min at 4°C. Beads were washed three times with PBS buffer.

4.8 | Protein detection by Western-blot

The mix of bead–protein complexes was finally eluted in denaturing loading buffer (XT sample buffer, Bio-Rad) and incubated for 10 min at 95°C. Proteins were separated on sodium dodecyl sulfate–polyacrylamide gel electrophoresis (SDS–PAGE) (4%–20% Pierce) and transferred onto a polyvinylidene diFluoride (PVDF) membrane (Thermo Fisher Scientific). The anti-PAN antibodies were raised against the purified recombinant protein from *P. horikoshii* (ProteoGenix) PAN was probed using a 1:5000 dilution and the antirabbit immunoglobulin G (IgG), horseradish peroxidase (HRP)-linked as secondary antibody (Amersham) with 1:10,000 dilution. For His-tagged proteins, Q9UZY3 was detected using anti-penta-His tag monoclonal antibody (Thermo Fisher Scientific) diluted at 1:2000 and the antimouse IgG, HRP-linked as secondary antibody (GE Healthcare). Proteins were revealed by immunofluorescence (Pierce™ ECL plus Western-Blotting Substrate, Thermo Fisher Scientific). Image acquisitions were done with a ChemiDoc XRS+ (Bio-Rad) and quantifications were carried out using ImageJ software (Schneider et al., 2012).

4.9 | Interactome analysis

The protein–protein interaction properties of Q9UZY3 were probed by pull-down experiments using the three purified His-tagged Q9UZY3 (Ntag, Ctag and ΔN-Ctag) incubated with 2 mg cell extract as described in Section 4.6. Negative controls were performed using cobalt-coated beads alone, instead of the bait–bead complexes. For the nucleic-acid free assays with Q9UZY3-Ntag and Q9UZY3-Ctag,

clarified cell extracts were incubated with a cocktail of 10 U RNase A (Roche), 100 U RNaseT1 (Thermo Fisher Scientific) and 10 U DNase I (Sigma) per milligram (mg) of extract for 30 min at 25°C. Experiments were done in duplicate for each His-tag position. Purified protein complexes were eluted in XT sample buffer (Bio-Rad) completed with reducing agent (Bio-Rad), incubated at 95°C for 10 min and separated by short migration on 12% SDS–PAGE (Criterion XT Precast gels, Bio-Rad). Protein-containing gel slices were submitted to shotgun proteomic analyses.

Samples were analyzed by mass spectrometry (MS) at the PAPPSO proteomics core facility (http://papso.inrae.fr) as described (Phung et al., 2020). Protein samples were injected twice into the MS instrument to make technical duplicates. Then peptides were identified with X!TandemPipeline software (Langella et al., 2017) by the spectrum-matching approach using the proteome database UP000009139 for *P. abyssi* proteins. The resulting specific spectra numbers reflected the signal of peptides specific for each protein. Data were normalized between replicates as described (Branson & Freitas, 2016). A minimal cut-off of two normalized specific spectra was applied as the minimum MS signal. The data of the two His-tagged Q9UZY3 (Ntag and Ctag) were merged to display redundant hit proteins. Diagram networks were created using Cytoscape 3.7.2 software (Shannon et al., 2003).

AUTHOR CONTRIBUTIONS

Gaëlle Hogrel contributed to experimental design, data collection and analysis and wrote the manuscript. Sébastien Laurent performed the pull-down experiments and analyzed LC/MS dataset. Gaëlle Hogrel, Ziad Ibrahim and Laura Marino-Puertas contributed to the protein cloning and purifications. Jacques Covès performed the PAN enzymatic assays and Laura Marino-Puertas proteasome degradation assays. Laura Marino-Puertas did the streptavidin pull-downs and ITC experiments. Daphna Fenel performed the microscopy analysis. Gaëlle Hogrel and Eric Girard crystallized and solved the structure. Gaëlle Hogrel and Frank Gabel collected and analyzed SAXS data. Marie-Claire Daugeron and Tamara Basta provided assistance with tRNA-binding assays. Didier Flament supervised interactome acquisition, data analysis and manuscript preparation. Marie-Claire Daugeron, Tamara Basta, Béatrice Clouet-d'Orval and Didier Flament were involved in the discussion and revised the manuscript. Bruno Franzetti conceived the study, acquired funding, wrote and revised the manuscript. All authors read and approved the final manuscript.

ACKNOWLEDGMENTS

We acknowledge financial support from the French Agence Nationale de la Recherche (grant [ANR-18-CE11-0018-01] to B.F. and [ANR-16-CE12-0016-01] to B.C.O). This work used the platforms of the Grenoble Instruct-ERIC Centre (ISBG: UMS 3518 CNRS-CEA-UGA-EMBL) with support from FRISBI (ANR-10-INBS-05-02) and GRAL, a project of the University Grenoble Alpes Graduate School (Ecoles Universitaires de Recherche) CBH-EUR-GS (ANR-17-EURE-0003) within the Grenoble Partnership for Structural Biology. The IBS Electron Microscope facility is supported by the Auvergne-Rhône-Alpes Region, the Fonds FEDER, the Fondation pour la Recherche Médicale and GIS-IBiSA. We acknowledge access to the European Synchrotron Radiation Facility (ESRF) facility, and we thank the beamline staff for their help. We also would like to thank Céline Henry and Lydie Correia of the PAPPSO proteomics core facility (http://papso.inra.fr) for the LC/MS analysis. We thank Caroline Mas for her help and advice with ITC. We are grateful to Clarisse Etienne, Aline Perquis, Valentina Geminian and Matteo Colombo for their initial work with PAN proteins. G.H. wants to thank Sylvain Engilberge for his precious support on the structural work of Pbp11 and Emilie Mahieu for the helpful discussions. IBS acknowledges integration into the Interdisciplinary Research Institute of Grenoble (IRIG, CEA).

CONFLICT OF INTEREST

The authors declare no conflict of interest.

ETHICS STATEMENT

The work presented here did not include human or animal subjects nor human or animal material or data. Thus, no formal consent or approval was necessary.

ACCESSION CODE

The coordinates and structure factors of the *P. abyssi* Pbp11 crystal structure have been deposited in the Protein Data Bank under accession code 7ANU. Supplementary Information accompanies this paper.

DATA AVAILABILITY STATEMENT

The data that support the findings of this study are available from the corresponding author upon reasonable request.

ORCID

Bruno Franzetti https://orcid.org/0000-0001-5323-0510

REFERENCES

Adams, P.D., Afonine, P.V., Bunkóczi, G., Chen, V.B., Davis, I.W., Echols, N. et al. (2010) PHENIX: a comprehensive python-based system for macromolecular structure solution. *Acta Crystallographica Section D: Biological Crystallography*, *66*(2), 213–221. https://doi.org/10.1107/S0907444909052925

Anjum, R.S., Bray, S.M., Blackwood, J.K., Kilkenny, M.L., Coelho, M.A., Foster, B.M. et al. (2015) Involvement of a eukaryotic-like ubiquitin-related modifier in the proteasome pathway of the archaeon *Sulfolobus acidocaldarius*. *Nature Communications*, *6*, 8163. https://doi.org/10.1038/ncomms9163

Arcus, V. (2002) OB-fold domains: a snapshot of the evolution of sequence, structure and function. *Current Opinion in Structural Biology*, *12*(6), 794–801. https://doi.org/10.1016/s0959-440x(02)00392-5

Ashburner, M., Ball, C.A., Blake, J.A., Botstein, D., Butler, H., Cherry, J.M. et al. (2000) Gene ontology: tool for the unification of biology. *Nature Genetics*, *25*(1), 25–29. https://doi.org/10.1038/75556

Borissenko, L. & Groll, M. (2005) Crystal structure of TET protease reveals complementary protein degradation pathways in prokaryotes. *Journal of Molecular Biology*, *346*(5), 1207–1219. https://doi.org/10.1016/j.jmb.2004.12.056

Branson, O.E. & Freitas, M.A. (2016) Tag-count analysis of large-scale proteomic data. *Journal of Proteome Research*, *15*(12), 4742–4746. https://doi.org/10.1021/acs.jproteome.6b00554

Burroughs, A.M., Balaji, S., Iyer, L.M. & Aravind, L. (2007) Small but versatile: the extraordinary functional and structural diversity of the beta-grasp fold. *Biology Direct*, *2*, 18. https://doi.org/10.1186/1745-6150-2-18

Chamieh, H., Guetta, D. & Franzetti, B. (2008) The two PAN ATPases from halobacterium display N-terminal heterogeneity and form labile complexes with the 20S proteasome. *The Biochemical Journal*, *411*(2), 387–397. https://doi.org/10.1042/BJ20071502

Cowtan, K. (2006) The Buccaneer software for automated model building. 1. Tracing protein chains. *Acta Crystallographica. Section D: Biological Crystallography*, *62*(Pt 9), 1002–1011. https://doi.org/10.1107/S0907444906022116

Cowtan, K.D. & Zhang, K.Y. (1999) Density modification for macromolecular phase improvement. *Progress in Biophysics and Molecular Biology*, *72*(3), 245–270. https://doi.org/10.1016/s0079-6107(99)00008-5

Defenouillère, Q. & Fromont-Racine, M. (2017) The ribosome-bound quality control complex: from aberrant peptide clearance to proteostasis maintenance. *Current Genetics*, *63*(6), 997–1005. https://doi.org/10.1007/s00294-017-0708-5

Defenouillère, Q., Yao, Y., Mouaikel, J., Namane, A., Galopier, A., Decourty, L. et al. (2013) Cdc48-associated complex bound to 60S particles is required for the clearance of aberrant translation products. *Proceedings of the National Academy of Sciences of the United States of America*, *110*(13), 5046–5051. https://doi.org/10.1073/pnas.1221724110

Di Tommaso, P., Moretti, S., Xenarios, I., Orobitg, M., Montanyola, A., Chang, J.-M. et al. (2011) T-coffee: a web server for the multiple sequence alignment of protein and RNA sequences using structural information and homology extension. *Nucleic Acids Research*, *39*(suppl_2), W13–W17. https://doi.org/10.1093/nar/gkr245

Dimitrova, L.N., Kuroha, K., Tatematsu, T. & Inada, T. (2009) Nascent peptide-dependent translation arrest leads to Not4p-mediated protein degradation by the proteasome. *The Journal of Biological Chemistry*, *284*(16), 10343–10352. https://doi.org/10.1074/jbc.M808840200

Doamekpor, S.K., Lee, J.-W., Hepowit, N.L., Wu, C., Charenton, C., Leonard, M. et al. (2016) Structure and function of the yeast listerin (Ltn1) conserved N-terminal domain in binding to stalled 60S ribosomal subunits. *Proceedings of the National Academy of Sciences of the United States of America*, *113*(29), E4151–E4160. https://doi.org/10.1073/pnas.1605951113

Doma, M.K. & Parker, R. (2006) Endonucleolytic cleavage of eukaryotic mRNAs with stalls in translation elongation. *Nature*, *440*(7083), 561–564. https://doi.org/10.1038/nature04530

Durá, M.A., Receveur-Brechot, V., Andrieu, J.-P., Ebel, C., Schoehn, G., Roussel, A. et al. (2005) Characterization of a TET-like aminopeptidase complex from the Hyperthermophilic archaeon *Pyrococcus horikoshii*. *Biochemistry*, *44*(9), 3477–3486. https://doi.org/10.1021/bi047736j

Emsley, P., Lohkamp, B., Scott, W.G. & Cowtan, K. (2010) Features and development of coot. *Acta Crystallographica. Section D: Biological Crystallography*, *66*(Pt 4), 486–501. https://doi.org/10.1107/S0907444910007493

Erauso, G., Reysenbach, A.-L., Godfroy, A., Meunier, J.-R., Crump, B., Partensky, F. et al. (1993) *Pyrococcus abyssi* sp. Nov., a new hyperthermophilic archaeon isolated from a deep-sea hydrothermal vent. *Archives of Microbiology*, *160*(5), 338–349. https://doi.org/10.1007/BF00252219

Evans, P. (2006) Scaling and assessment of data quality. *Acta Crystallographica. Section D: Biological Crystallography*, *62*(Pt 1), 72–82. https://doi.org/10.1107/S0907444905036693

Finley, D., Ciechanover, A. & Varshavsky, A. (2004) Ubiquitin as a central cellular regulator. *Cell*, *116*(2 Suppl), S29–S32, 2 p following S32. https://doi.org/10.1016/s0092-8674(03)00971-1

Finley, D. & Prado, M.A. (2020) The proteasome and its network: engineering for adaptability. *Cold Spring Harbor Perspectives in Biology*, *12*(1), a033985. https://doi.org/10.1101/cshperspect.a033985

Franke, D., Petoukhov, M.V., Konarev, P.V., Panjkovich, A., Tuukkanen, A., Mertens, H.D.T. et al. (2017) ATSAS 2.8: a comprehensive data analysis suite for small-angle scattering from macromolecular solutions. *Journal of Applied Crystallography*, *50*(4), 1212–1225. https://doi.org/10.1107/S1600576717007786

Frischmeyer, P.A., van Hoof, A., O'Donnell, K., Guerrerio, A.L., Parker, R. & Dietz, H.C. (2002) An mRNA surveillance mechanism that eliminates transcripts lacking termination codons. *Science (New York, N.Y.)*, *295*(5563), 2258–2261. https://doi.org/10.1126/science.1067338

Gasteiger, E., Hoogland, C., Gattiker, A., Duvaud, S., Wilkins, M. R., Appel, R. D., & Bairoch, A. (2005) Protein identification and analysis tools on the ExPASy server. In: J. M. Walker (Éd.) *The proteomics protocols handbook*. Totowa, NJ: Humana Press, pp. 571–607. https://doi.org/10.1385/1-59259-890-0:571

The Gene Ontology Consortium. (2019) The gene ontology resource: 20 years and still GOing strong. *Nucleic Acids Research*, *47*(D1), D330–D338. https://doi.org/10.1093/nar/gky1055

Goldberg, A.L. (2003) Protein degradation and protection against misfolded or damaged proteins. *Nature*, *426*(6968), 895–899. https://doi.org/10.1038/nature02263

Groll, M., Brandstetter, H., Bartunik, H., Bourenkow, G. & Huber, R. (2003) Investigations on the maturation and regulation of archaebacterial proteasomes. *Journal of Molecular Biology*, *327*(1), 75–83. https://doi.org/10.1016/s0022-2836(03)00080-9

Hajizadeh, N.R., Franke, D., Jeffries, C.M. & Svergun, D.I. (2018) Consensus Bayesian assessment of protein molecular mass from solution X-ray scattering data. *Scientific Reports*, *8*(1), 7204. https://doi.org/10.1038/s41598-018-25355-2

Hennell James, R., Caceres, E.F., Escasinas, A., Alhasan, H., Howard, J.A., Deery, M.J. et al. (2017) Functional reconstruction of a eukaryotic-like E1/E2/(RING) E3 ubiquitylation cascade from an uncultured archaeon. *Nature Communications*, *8*(1), 1120. https://doi.org/10.1038/s41467-017-01162-7

Holm, L. (2020) DALI and the persistence of protein shape. *Protein Science: A Publication of the Protein Society*, *29*(1), 128–140. https://doi.org/10.1002/pro.3749

Holst, M. & Saied, F. (1993) Multigrid solution of the Poisson—Boltzmann equation. *Journal of Computational Chemistry*, *14*(1), 105–113. https://doi.org/10.1002/jcc.540140114

Humbard, M.A., Miranda, H.V., Lim, J.-M., Krause, D.J., Pritz, J.R., Zhou, G. et al. (2010) Ubiquitin-like small archaeal modifier proteins (SAMPs) in *Haloferax volcanii*. *Nature*, *463*(7277), 54–60. https://doi.org/10.1038/nature08659

Ibrahim, Z., Martel, A., Moulin, M., Kim, H.S., Härtlein, M., Franzetti, B. et al. (2017) Time-resolved neutron scattering provides new insight into protein substrate processing by a AAA+ unfoldase. *Scientific Reports*, *7*, 40948. https://doi.org/10.1038/srep40948

Ito-Harashima, S., Kuroha, K., Tatematsu, T. & Inada, T. (2007) Translation of the poly(a) tail plays crucial roles in nonstop mRNA surveillance via translation repression and protein destabilization by proteasome in yeast. *Genes & Development*, *21*(5), 519–524. https://doi.org/10.1101/gad.1490207

Kabsch, W. (2010) XDS. *Acta Crystallographica. Section D: Biological Crystallography*, *66*(Pt 2), 125–132. https://doi.org/10.1107/S0907444909047337

Karamyshev, A.L. & Karamysheva, Z.N. (2018) Lost in translation: ribosome-associated mRNA and protein quality controls. *Frontiers in Genetics*, *9*, 431. https://doi.org/10.3389/fgene.2018.00431

Kelley, L.A., Mezulis, S., Yates, C.M., Wass, M.N. & Sternberg, M.J.E. (2015) The Phyre2 web portal for protein modeling, prediction and analysis. *Nature Protocols*, *10*(6), 845–858. https://doi.org/10.1038/nprot.2015.053

Kim, Y.-C., Snoberger, A., Schupp, J. & Smith, D.M. (2015) ATP binding to neighbouring subunits and intersubunit allosteric coupling underlie proteasomal ATPase function. *Nature Communications*, *6*, 8520. https://doi.org/10.1038/ncomms9520

Koonin, E.V., Wolf, Y.I. & Aravind, L. (2001) Prediction of the archaeal exosome and its connections with the proteasome and the translation and transcription machineries by a comparative-genomic approach. *Genome Research*, *11*(2), 240–252. https://doi.org/10.1101/gr.162001

Kumoi, K., Satoh, T., Murata, K., Hiromoto, T., Mizushima, T., Kamiya, Y. et al. (2013) An archaeal homolog of proteasome assembly factor functions as a proteasome activator. *PLoS One*, *8*(3), e60294. https://doi.org/10.1371/journal.pone.0060294

Kusmierczyk, A.R., Kunjappu, M.J., Kim, R.Y. & Hochstrasser, M. (2011) A conserved 20S proteasome assembly factor requires a C-terminal HbYX motif for proteasomal precursor binding. *Nature Structural & Molecular Biology*, *18*(5), 622–629. https://doi.org/10.1038/nsmb.2027

Langella, O., Valot, B., Balliau, T., Blein-Nicolas, M., Bonhomme, L. & Zivy, M. (2017) X!TandemPipeline: a tool to manage sequence redundancy for protein inference and Phosphosite identification. *Journal of Proteome Research*, *16*(2), 494–503. https://doi.org/10.1021/acs.jproteome.6b00632

Lytvynenko, I., Paternoga, H., Thrun, A., Balke, A., Müller, T.A., Chiang, C.H. et al. (2019) Alanine tails signal proteolysis in bacterial ribosome-associated quality control. *Cell*, *178*(1), 76–90.e22. https://doi.org/10.1016/j.cell.2019.05.002

Mahieu, E., Covès, J., Krüger, G., Martel, A., Moulin, M., Carl, N. et al. (2020) Observing protein degradation by the PAN-20S proteasome by time-resolved neutron scattering. *Biophysical Journal*, *119*(2), 375–388. https://doi.org/10.1016/j.bpj.2020.06.015

Majumder, P. & Baumeister, W. (2019) Proteasomes: unfoldase-assisted protein degradation machines. *Biological Chemistry*, *401*(1), 183–199. https://doi.org/10.1515/hsz-2019-0344

Majumder, P., Rudack, T., Beck, F., Danev, R., Pfeifer, G., Nagy, I. et al. (2019) Cryo-EM structures of the archaeal PAN-proteasome reveal an around-the-ring ATPase cycle. *Proceedings of the National Academy of Sciences of the United States of America*, *116*(2), 534–539. https://doi.org/10.1073/pnas.1817752116

Maupin-Furlow, J. (2011) Proteasomes and protein conjugation across domains of life. *Nature Reviews. Microbiology*, *10*(2), 100–111. https://doi.org/10.1038/nrmicro2696

Maupin-Furlow, J.A. (2013a) Archaeal proteasomes and sampylation. *Sub-cellular Biochemistry*, *66*, 297–327. https://doi.org/10.1007/978-94-007-5940-4_11

Maupin-Furlow, J.A. (2013b) Ubiquitin-like proteins and their roles in archaea. *Trends in Microbiology*, *21*(1), 31–38. https://doi.org/10.1016/j.tim.2012.09.006

McCoy, A.J., Grosse-Kunstleve, R.W., Adams, P.D., Winn, M.D., Storoni, L.C. & Read, R.J. (2007) Phaser crystallographic software. *Journal of Applied Crystallography*, *40*(4), 658–674. https://doi.org/10.1107/S0021889807021206

Murzin, A.G. (1993) OB(oligonucleotide/oligosaccharide binding)-fold: common structural and functional solution for non-homologous sequences. *The EMBO Journal*, *12*(3), 861–867.

Navon, A. & Ciechanover, A. (2009) The 26 S proteasome: from basic mechanisms to drug targeting. *The Journal of Biological Chemistry*, *284*(49), 33713–33718. https://doi.org/10.1074/jbc.R109.018481

Nissen, P., Kjeldgaard, M., Thirup, S., Polekhina, G., Reshetnikova, L., Clark, B.F. et al. (1995) Crystal structure of the ternary complex of Phe-tRNAPhe, EF-Tu, and a GTP analog. *Science (New York, N.Y.)*, *270*(5241), 1464–1472. https://doi.org/10.1126/science.270.5241.1464

Nissen, P., Thirup, S., Kjeldgaard, M. & Nyborg, J. (1999) The crystal structure of Cys-tRNACys–EF-Tu–GDPNP reveals general and specific features in the ternary complex and in tRNA. *Structure*, *7*(2), 143–156. https://doi.org/10.1016/S0969-2126(99)80021-5

Notredame, C., Higgins, D.G. & Heringa, J. (2000) T-coffee: a novel method for fast and accurate multiple sequence alignment. *Journal of Molecular Biology*, *302*(1), 205–217. https://doi.org/10.1006/jmbi.2000.4042

Perrochia, L., Guetta, D., Hecker, A., Forterre, P. & Basta, T. (2013) Functional assignment of KEOPS/EKC complex subunits in the biosynthesis of the universal t6A tRNA modification. *Nucleic Acids Research*, *41*(20), 9484–9499. https://doi.org/10.1093/nar/gkt720

Phung, D.K., Etienne, C., Batista, M., Langendijk-Genevaux, P., Moalic, Y., Laurent, S. et al. (2020) RNA processing machineries in archaea: the 5′-3′ exoribonuclease aRNase J of the β-CASP family is engaged specifically with the helicase ASH-Ski2 and the 3′-5′ exoribonucleolytic RNA exosome machinery. *Nucleic Acids Research*, *48*(7), 3832–3847. https://doi.org/10.1093/nar/gkaa052

Pluchon, P.-F., Fouqueau, T., Crezé, C., Laurent, S., Briffotaux, J., Hogrel, G. et al. (2013) An extended network of genomic maintenance in the archaeon *Pyrococcus abyssi* highlights unexpected associations between eucaryotic homologs. *PLoS One*, *8*(11), e79707. https://doi.org/10.1371/journal.pone.0079707

Ranjan, N., Damberger, F.F., Sutter, M., Allain, F.H.-T. & Weber-Ban, E. (2011) Solution structure and activation mechanism of ubiquitin-like small archaeal modifier proteins. *Journal of Molecular Biology*, *405*(4), 1040–1055. https://doi.org/10.1016/j.jmb.2010.11.040

Risa, G.T., Hurtig, F., Bray, S., Hafner, A.E., Harker-Kirschneck, L., Faull, P. et al. (2020) The proteasome controls ESCRT-III–mediated cell division in an archaeon. *Science*, *369*(6504), eaaz2532. https://doi.org/10.1126/science.aaz2532

Robert, X. & Gouet, P. (2014) Deciphering key features in protein structures with the new ENDscript server. *Nucleic Acids Research*, *42*(W1), W320–W324. https://doi.org/10.1093/nar/gku316

Schneider, C.A., Rasband, W.S. & Eliceiri, K.W. (2012) NIH image to ImageJ: 25 years of image analysis. *Nature Methods*, *9*(7), 671–675. https://doi.org/10.1038/nmeth.2089

Sha, Z., Brill, L.M., Cabrera, R., Kleifeld, O., Scheliga, J.S., Glickman, M.H. et al. (2009) The eIF3 interactome reveals the translasome, a supercomplex linking protein synthesis and degradation machineries. *Molecular Cell*, *36*(1), 141–152. https://doi.org/10.1016/j.molcel.2009.09.026

Shannon, P., Markiel, A., Ozier, O., Baliga, N.S., Wang, J.T., Ramage, D. et al. (2003) Cytoscape: a software environment for integrated models of biomolecular interaction networks. *Genome Research*, *13*(11), 2498–2504. https://doi.org/10.1101/gr.1239303

Smith, D.M., Fraga, H., Reis, C., Kafri, G. & Goldberg, A.L. (2011) ATP binds to proteasomal ATPases in pairs with distinct functional effects, implying an ordered reaction cycle. *Cell*, *144*(4), 526–538. https://doi.org/10.1016/j.cell.2011.02.005

Theobald, D.L., Mitton-Fry, R.M. & Wuttke, D.S. (2003) Nucleic acid recognition by OB-fold proteins. *Annual Review of Biophysics and Biomolecular Structure*, *32*, 115–133. https://doi.org/10.1146/annurev.biophys.32.110601.142506

van Hoof, A., Frischmeyer, P.A., Dietz, H.C. & Parker, R. (2002) Exosome-mediated recognition and degradation of mRNAs lacking a termination codon. *Science (New York, N.Y.)*, *295*(5563), 2262–2264. https://doi.org/10.1126/science.1067272

Wang, F., Durfee, L.A. & Huibregtse, J.M. (2013) A cotranslational ubiquitination pathway for quality control of misfolded proteins. *Molecular Cell*, *50*(3), 368–378. https://doi.org/10.1016/j.molcel.2013.03.009

Wilson, H.L., Ou, M.S., Aldrich, H.C. & Maupin-Furlow, J. (2000) Biochemical and physical properties of the *Methanococcus*

jannaschii 20S proteasome and PAN, a homolog of the ATPase (Rpt) subunits of the eucaryal 26S proteasome. *Journal of Bacteriology*, *182*(6), 1680–1692. https://doi.org/10.1128/jb.182.6.1680-1692.2000

Zwickl, P., Ng, D., Woo, K.M., Klenk, H.P. & Goldberg, A.L. (1999) An archaebacterial ATPase, homologous to ATPases in the eukaryotic 26 S proteasome, activates protein breakdown by 20 S proteasomes. *The Journal of Biological Chemistry*, *274*(37), 26008–26014. https://doi.org/10.1074/jbc.274.37.26008

SUPPORTING INFORMATION

Additional supporting information may be found in the online version of the article at the publisher's website.

How to cite this article: Hogrel, G., Marino-Puertas, L., Laurent, S., Ibrahim, Z., Covès, J., Girard, E., Gabel, F., Fenel, D., Daugeron, M-C, Clouet-d'Orval, B., Basta, T., Flament, D. & Franzetti, B. (2022). Characterization of a small tRNA-binding protein that interacts with the archaeal proteasome complex. *Molecular Microbiology*, *118*, 16–29. https://doi.org/10.1111/mmi.14948